Title

Molecular dissection of the mechanism by which EWS/FLI expression compromises actin cytoskeletal integrity and cell adhesion in Ewing sarcoma

Journal

Molecular Biology of the Cell, 25(18)

ISSN

1059-1524

Authors

Chaturvedi, Aashi
Hoffman, Laura M
Jensen, Christopher C
et al.

Publication Date

2014-09-15

DOI

10.1091/mbc.e14-01-0007

Peer reviewed

Molecular dissection of the mechanism by which EWS/FLI expression compromises actin cytoskeletal integrity and cell adhesion in Ewing sarcoma

Aashi Chaturvedi[a,b,*], Laura M. Hoffman[a,c,*], Christopher C. Jensen[a], Yi-Chun Lin[a,b], Allie H. Grossmann[d], R. Lor Randall[e,f], Stephen L. Lessnick[a,b,e], Alana L. Welm[a,b], and Mary C. Beckerle[a,b,c]

[a]Huntsman Cancer Institute, [b]Department of Oncological Sciences, [c]Department of Biology, [d]Department of Pathology, and [f]Department of Orthopaedics, Sarcoma Services, Huntsman Cancer Institute, University of Utah, Salt Lake City, UT 84112; [e]Center for Children's Cancer Research, Huntsman Cancer Institute, Division of Pediatric Hematology/Oncology, University of Utah School of Medicine, Salt Lake City, UT 84132

ABSTRACT **Ewing sarcoma is the second-most-common bone cancer in children. Driven by an oncogenic chromosomal translocation that results in the expression of an aberrant transcription factor, EWS/FLI, the disease is typically aggressive and micrometastatic upon presentation. Silencing of EWS/FLI in patient-derived tumor cells results in the altered expression of hundreds to thousands of genes and is accompanied by dramatic morphological changes in cytoarchitecture and adhesion. Genes encoding focal adhesion, extracellular matrix, and actin regulatory proteins are dominant targets of EWS/FLI-mediated transcriptional repression. Reexpression of genes encoding just two of these proteins, zyxin and α5 integrin, is sufficient to restore cell adhesion and actin cytoskeletal integrity comparable to what is observed when the EWS/FLI oncogene expression is compromised. Using an orthotopic xenograft model, we show that EWS/FLI-induced repression of α5 integrin and zyxin expression promotes tumor progression by supporting anchorage-independent cell growth. This selective advantage is paired with a tradeoff in which metastatic lung colonization is compromised.**

Monitoring Editor
Paul Forscher
Yale University

Received: Jan 3, 2014
Revised: Jun 27, 2014
Accepted: Jul 15, 2014

INTRODUCTION

Ewing sarcoma is a round-cell malignant neoplasm of the bone that typically affects adolescents and young adults. It usually develops in the diaphysis or metaphysis of long bones, most commonly in the femur, tibia, and humerus (Kimber *et al.*, 1998; Spraker *et al.*, 2012). Ewing sarcoma is an aggressive cancer that grows rapidly and metastasizes to lungs and bones (Karosas, 2010). Treatment of apparently localized primary tumors involves chemotherapy and surgery and/or radiation therapy. Despite these interventions, many patients relapse even after definitive local control of the primary tumor, illustrating the fact that most patients have occult disseminated disease upon presentation (McAllister and Lessnick, 2005; Spraker *et al.*, 2012). Patients with metastatic or recurrent disease face poor prognosis, with <15% 5-yr survival rate. Knowledge of the molecular mechanisms that determine Ewing sarcoma cell behavior will be crucial in understanding disease progression and ultimately intervening with targeted treatment.

Ewing sarcoma is caused by a reciprocal chromosomal translocation involving a portion of the *EWSR1* gene on chromosome 22 and genes encoding members of the ETS family of transcription factors, most commonly *FLI1*, which maps to chromosome 11 (Turc-Carel *et al.*, 1988; Delattre *et al.*, 1992; Sankar and Lessnick, 2011). In ~85% of cases, a t(11;22)(q24;q12) translocation results in the

This article was published online ahead of print in MBoC in Press (http://www.molbiolcell.org/cgi/doi/10.1091/mbc.E14-01-0007) on July 23, 2014.

*These authors contributed equally to this work.

Address correspondence to: Mary C. Beckerle (mary.beckerle@hci.utah.edu).

Abbreviations used: CD99, cell surface protein that is a marker for Ewing sarcoma; EWS/FLI, oncogenic fusion protein t(11;22) in Ewing sarcoma; EWSR1, target gene on chromosome 22; FLI1, target gene on chromosome 11.

expression of a chimeric transcription factor in which a strong transcription regulatory domain found in EWS is fused to a portion of FLI that includes a DNA-binding domain (Aurias *et al.*, 1984; Delattre *et al.*, 1992; Lessnick *et al.*, 1995; May *et al.*, 1993a). EWS/FLI acts as a master transcriptional regulator that modulates the expression of a large number of genes. Several up-regulated targets of EWS/FLI have been extensively studied, including NKX2.2, NR0B1, and Caveolin1 (Kinsey *et al.*, 2006; Tirado *et al.*, 2006; Owen *et al.*, 2008). Although predicted to aberrantly activate transcription, EWS/FLI also causes repression of hundreds to thousands of genes (Kinsey *et al.*, 2006; Smith *et al.*, 2006; Owen *et al.*, 2008). With a few exceptions (Mateo-Lozano *et al.*, 2003; Herrero-Martin *et al.*, 2009; Borinstein *et al.*, 2011), the down-regulated targets of EWS/FLI have not been extensively characterized. However, recent work provides evidence that a key mode of oncogenic transformation by EWS/FLI involves repression of specific gene expression (Sankar *et al.*, 2013a). Understanding the targets and effect of EWS/FLI-dependent transcriptional repression is thus a key imperative in dissection of the pathogenesis of Ewing sarcoma.

Recent studies suggest that EWS/FLI is not only required for tumorigenesis (Smith *et al.*, 2006), but it also modulates key cellular properties such as cell adhesion, motility, and invasion (Chaturvedi *et al.*, 2012). For example, RNA interference–based knockdown of EWS/FLI expression in human Ewing sarcoma cells revealed that EWS/FLI promotes loss of cytoskeletal integrity as well as reduced tumor cell adhesion and spreading (Chaturvedi *et al.*, 2012). The dramatic effect of the transforming oncogene EWS/FLI on cell architecture and adhesion could provide a mechanism to couple unregulated cell growth to phenotypic changes that promote sarcoma metastasis, perhaps explaining why Ewing sarcoma displays such early metastatic behavior. In theory, the aberrant regulation of adhesion genes by EWS/FLI could affect multiple stages of Ewing sarcoma metastasis: initial tumor cell release and dissemination, extravasation, and second-site adhesion/colonization.

Here we analyze the gene expression changes associated with knockdown of EWS/FLI expression in human Ewing sarcoma cells, with the goal of interrogating the mechanisms underlying the dramatic alterations in cytoskeleton and cell adhesion that accompany transformation by EWS/FLI. We find that the top three classes of genes that are repressed by EWS/FLI expression are categorized as genes related to structure or function of focal adhesions, extracellular matrix (ECM)–receptor interactions, and regulation of the actin cytoskeleton. By genetic reconstitution experiments, we identified zyxin and α5 integrin as two EWS/FLI target genes that, when reexpressed in Ewing sarcoma cells, are sufficient to induce a dramatic restoration of actin cytoarchitecture and cell adhesion. We extend the results from cell biology studies into an experimental mouse model that effectively recapitulates the clinical manifestations of Ewing sarcoma observed in patients, including rapid formation of osteolytic tumors and aggressive metastasis to lungs and other bones. Our results highlight the importance of misregulation of adhesion and cytoskeletal regulation for Ewing sarcoma tumor phenotype. In addition, our findings suggest that misregulation of genes within tumors can alternately provide selective advantages or disadvantages, depending on the specific context. Our results illustrate that not all gene expression changes that are promoted by transforming oncogenes are advantageous for all aspects of a tumor's life history, but instead that the changes may be enabling for one aspect, such as supporting anchorage-independent cell growth, even as they may compromise the ability of the tumor cells to establish colonies at second sites.

RESULTS

EWS/FLI expression compromises the cytoskeleton of Ewing sarcoma cells

The cell of origin that gives rise to Ewing sarcoma has not been definitively identified (Ewing, 1921; Cavazzana *et al.*, 1987; Kovar, 2005; Tirode *et al.*, 2007; Jedlicka, 2010). Consequently, the approach of ectopic EWS/FLI expression as a way to model oncogene effect on cell behavior is fraught with difficulty, owing to the uncertain effect of inappropriate cellular context (Braunreiter *et al.*, 2006; Owen and Lessnick, 2006). To circumvent this challenge, we studied how the EWS/FLI oncoprotein influences cellular behavior by using an RNA interference (RNAi) approach to knock down EWS/FLI expression in patient-derived Ewing sarcoma cells (A673 and EWS502).

We used retrovirally encoded short hairpin RNA directed against EWS/FLI transcripts to knock down the expression of EWS/FLI (EWS/FLI RNAi), with RNAi against luciferase serving as our control RNAi, and compared the resulting alterations in cellular behavior. We reported previously that knockdown of EWS/FLI expression in multiple human Ewing sarcoma cell lines resulted in dramatic effects on cell phenotype, including alterations in adhesion and motility (Chaturvedi *et al.*, 2012). In an effort to mimic the extracellular matrix context found within bone, the site of Ewing sarcoma genesis, we examined the behavior of cells plated on fibronectin, an extracellular matrix protein that is prominent in bone (Rodan and Rodan, 1997). As can be seen in Figure 1A, Ewing sarcoma cells displayed a profound cytoskeletal deficit when cultured on a fibronectin matrix. The A673 cells appeared small and poorly spread, with thin and short actin stress fibers. In contrast, when EWS/FLI expression was knocked down by RNAi, the Ewing sarcoma cells underwent a dramatic morphological transformation in which they exhibited pronounced adhesion and spreading to the fibronectin substratum and displayed robust actin stress fibers. These results illustrated the effect of EWS/FLI expression on adhesion and cytoarchitecture and prompted us to explore the mechanism by which EWS/FLI influences these phenotypic attributes of Ewing sarcoma cells.

EWS/FLI targets gene expression of many adhesion-related genes

EWS/FLI is an oncogenic transcription factor that modulates the expression of hundreds to thousands of genes (Owen *et al.*, 2008). To identify candidate targets of EWS/FLI that might influence adhesion and cytoarchitecture, we analyzed a previously published microarray analysis of EWS/FLI-regulated genes (Owen *et al.*, 2008). Selection of genes whose expression was decreased at least 1.8-fold by EWS/FLI revealed 222 genes that were down-regulated by EWS/FLI by this criterion. Kyoto Encyclopedia of Genes and Genomes (KEGG) analysis revealed that the top three classes of genes down-regulated by EWS/FLI were those encoding focal adhesion proteins, modulators of extracellular matrix–receptor interactions, and regulators of the actin cytoskeleton (Table 1), consistent with the major cellular phenotypes we observed in Ewing sarcoma cells (Figure 1A; Chaturvedi *et al.*, 2012). Inspection of the EWS/FLI down-regulated genes revealed that more than one-third would be expected to influence the actin cytoskeleton, cell–matrix communication, or cell adhesion and migration based on their annotated functions (Supplemental Table S1). The largest single class of genes down-regulated by EWS/FLI expression encode focal adhesion proteins. Focal adhesions are regions of the cell surface specialized for cell–matrix adhesion and transmembrane communication, known to convey information about extracellular matrix composition, as well as mechanical

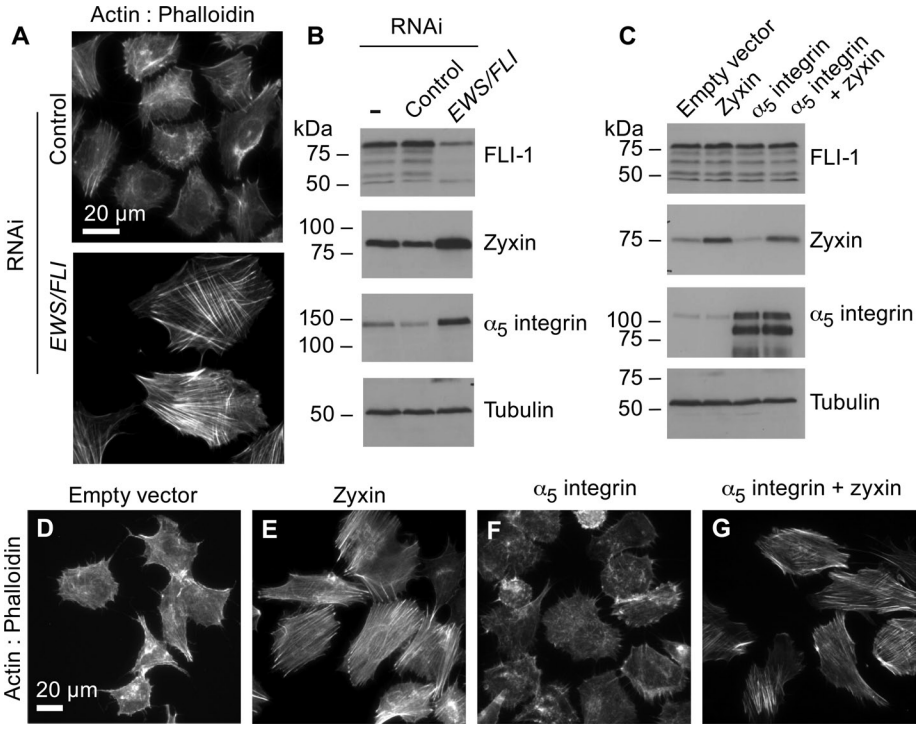

FIGURE 1: EWS/FLI-dependent changes in the actin cytoskeleton and contributions of cytoskeletal regulators. (A) Widefield fluorescence images of A673 Ewing sarcoma cells stained with phalloidin to visualize the actin filament network. A673 cells with EWS/FLI RNAi had robust actin cytoskeletons and were more spread than A673 cells with control RNAi. Scale bar, 20 μm. (B) Western immunoblot of parent Ewing sarcoma A673 cells (lane 1), A673 cells with control RNAi (lane 2), or EWS/FLI RNAi (lane 3) were probed with antibodies for FLI-1, zyxin, α5 integrin, and tubulin (loading control). EWS/FLI knockdown resulted in increased zyxin and α5 integrin protein. (C) Western immunoblot of Ewing sarcoma cells engineered to express empty vector, zyxin, α5 integrin, or both α5 integrin and zyxin were probed with antibodies for FLI-1, zyxin, α5 integrin, and tubulin (loading control). Independent expression of zyxin or α5 integrin above the endogenous levels in A673 cells did not affect the level of the other protein. (D–G) Widefield fluorescence images of phalloidin-stained A673 cells engineered to express empty vector (D), zyxin (E), α5 integrin (F), or both α5 integrin and zyxin (G) suggest increased actin cytoskeleton and cell spreading in cells that reexpress these proteins.

stress to the cell interior. Focal adhesions are themselves complex multicomponent structures, with >100 known protein constituents (Zaidel-Bar *et al.*, 2007; Geiger and Yamada, 2011).

From the list of genes that are down-regulated by EWS/FLI, we selected the genes encoding zyxin and α5 integrin for further study because of their known influence on cytoskeleton and cell–matrix interactions. Zyxin is an evolutionarily conserved regulator of the actin cytoskeleton that is required for maintenance and repair of actin stress fibers (Yoshigi *et al.*, 2005; Smith *et al.*, 2010; Hoffman *et al.*, 2012). Zyxin was previously shown to be down-regulated when EWS/FLI is expressed in 3T3 fibroblasts, illustrating that EWS/FLI repression of zyxin expression occurs in multiple cellular contexts (Amsellem *et al.*, 2005). Integrins are transmembrane αβ heterodimeric receptors for extracellular matrix that are critical for cell–substratum adhesion, as well as for stress fiber anchorage and integrity (Lotz *et al.*, 2000; Hynes, 2002; Campbell and Humphries, 2011). The α5 integrin is a known modulator of cell adhesion, migration, and cell–matrix communication that dimerizes with β1 integrin subunit to confer adhesion to fibronectin (Mostafavi-Pour *et al.*, 2003; Margadant *et al.*, 2011; Gupton *et al.*, 2012; Nagae *et al.*, 2012). Fibronectin expression is also reduced in EWS/FLI-transformed cells (Supplemental Table S1), consistent with the proposal that the EWS/FLI oncogene acts, at least in part, by abrogating cell–matrix adhesion and the associated actin cytoskeleton.

Validating the microarray findings, Western immunoblot analysis comparing the protein complements in control and EWS/FLI-knockdown cells revealed that both zyxin and α5 integrin are down-regulated by EWS/FLI expression (Figure 1B). Evidence that the RNAi was effective in abrogating EWS/FLI expression is shown in Figure 1B, in which FLI-1 antibody detects reduced EWS/FLI fusion protein. Tubulin expression serves as a surrogate for cell number and controls for equivalent sample loading in this experiment.

Reexpression of zyxin and α5 integrin in Ewing sarcoma cells influences the actin cytoskeleton, cell adhesion, and spreading

To study the effect of reduced expression of zyxin and α5 integrin in Ewing sarcoma, we reexpressed these down-regulated targets in patient-derived Ewing sarcoma cells using retrovirus to program the cells to express these cDNAs of interest. As can be seen in Figure 1C, by Western immunoblot analysis, we observe increases in zyxin and/or α5 integrin expression in the reprogrammed cells. Expression of these proteins does not detectably alter the levels of EWS/FLI in the cells, as detected with anti-FLI1 antibody.

Although EWS/FLI affects the expression of hundreds to thousands of genes, the reexpression of just one or two of these, zyxin and/or α5 integrin, in the Ewing sarcoma cells resulted in dramatic phenotypic alterations in the cells. Of importance, the individual expression of zyxin and α5 integrin induced distinct alterations in morphology and cytoarchitecture of the Ewing sarcoma cells. Compared to the parental A673 cells infected with the empty retroviral vector, which were poorly spread and exhibited only rudimentary stress fibers (Figure 1D), Ewing sarcoma cells programmed to express zyxin displayed a profound elaboration of actin stress fibers, with an increase in cell spreading as well (Figure 1E). Expression of α5 integrin alone appeared to improve cell spreading without resulting in enhancement of actin cytoskeletal arrays (Figure 1F). When these proteins were coexpressed, the Ewing sarcoma cells were marked by both well-formed actin stress fibers and enhanced cell spreading (Figure 1G). Expression of zyxin and/or α5 integrin in a second Ewing sarcoma cell line, EWS502 cells, also resulted in a more organized actin cytoskeleton with enhanced cell spreading (Supplemental Figure S1).

Higher magnification and quantitative analysis of these initial findings confirmed the significant and unique effects of zyxin and α5 integrin on Ewing sarcoma cell morphology and cytoarchitecture (Figure 2). The cells were double labeled with phalloidin to visualize filamentous actin (Figure 2, A–D) and anti-paxillin antibody to mark focal adhesions (Figure 2, E–H). The size (Figure 2I) and number (Figure 2J) of focal adhesions were quantitated for each experimental condition. Knockdown of EWS/FLI expression in Ewing sarcoma cells resulted in a statistically significant increase in the average focal

	KEGG pathway	Number of genes	Gene set	*z*-score
1	Focal adhesion	24	190	8.5
2	ECM–receptor interaction	14	80	8.1
3	Regulation of actin cytoskeleton	13	187	3.6
4	Amoebiasis	12	100	5.7
5	Protein processing in endoplasmic reticulum	12	144	4.2
6	Lysosome	10	109	4.1
7	Phagosome	9	139	2.7
8	Arrhythmogenic right ventricular cardiomyopathy (ARVC)	8	68	4.6
9	Cell adhesion molecules (CAMs)	8	116	2.8
10	Antigen processing and presentation	7	61	4.2
11	Natural killer cell–mediated cytotoxicity	7	117	2.2
12	Protein digestion and absorption	7	70	3.7
13	Toxoplasmosis	7	118	2.1
14	Viral myocarditis	7	65	4.0
15	Adherens junction	6	71	3.0
16	Bacterial invasion of epithelial cells	6	64	3.3
17	Dilated cardiomyopathy	6	82	2.5
18	Hypertrophic cardiomyopathy (HCM)	6	79	2.7
19	Small-cell lung cancer	6	83	2.5
20	Complement and coagulation cascades	5	67	2.4
21	Prion diseases	5	34	4.3
22	Shigellosis	5	55	2.9
23	Allograft rejection	4	32	3.4
24	Amino sugar and nucleotide sugar metabolism	4	42	2.7
25	Autoimmune thyroid disease	4	48	2.4
26	Bladder cancer	4	41	2.8
27	Graft-versus-host disease	4	33	3.3
28	NOD-like receptor signaling pathway	4	54	2.1
29	Type I diabetes mellitus	4	37	3.0
30	Glycosaminoglycan biosynthesis–chondroitin sulfate	2	16	2.4
31	Glycosaminoglycan degradation	2	18	2.2

KEGG pathway groups of genes that are down-regulated at least 1.8-fold by EWS/FLI. The top three categories modulated by EWS/FLI are genes encoding focal adhesion–related proteins, ECM and receptor interaction proteins, and regulators of the actin cytoskeleton. The KEGG analysis therefore suggests the importance of cell adhesion and cytoskeletal pathways and components for EWS/FLI-dependent changes in Ewing sarcoma.

TABLE 1: Categories of down-regulated target genes of EWS/FLI oncoprotein.

adhesion size from 1.3 to 1.8 μm^2 (Figure 2I). Reexpression of either zyxin, α5 integrin, or both zyxin and α5 integrin restored the size of paxillin-rich focal adhesions to a level that is not statistically different from what is observed when EWS/FLI is knocked down in Ewing sarcoma cells by RNAi (Figure 2I).

Ewing sarcoma cells or those with control RNAi displayed fewer focal adhesions (~50/cell) than cells in which EWS/FLI expression was knocked down, which exhibited an average of 177 focal adhesions/cell (Figure 2J). Expression of zyxin and/or α5 integrin in Ewing sarcoma cells resulted in a statistically significant increase of focal adhesion number (Figure 2J). Of interest, however, zyxin expression had a more profound effect on focal adhesion number than did expression of α5 integrin. For example, expression of α5 integrin led to moderate increase in number of focal adhesions from an average of 50 to 70 per cell (Figure 2J). However, expression of zyxin alone or with α5 integrin led to dramatic increase in the focal adhesion number to >150 focal adhesions/cell (Figure 2J), highlighting the differential effect of zyxin and α5 integrin on focal adhesion number.

Given the established link between focal adhesion development and cell spreading (Smilenov *et al.*, 1999; Salsmann *et al.*, 2006), the increased focal adhesion size and number observed upon reexpression of zyxin and/or α5 integrin was consistent with low-magnification analysis, which suggested that reexpression of either zyxin or α5 integrin enhanced cell spreading. To examine this possibility quantitatively, we measured the areas of phalloidin-stained cells (e.g., cells such as those represented in Figure 2, A–D). Expression of zyxin and/or α5 integrin resulted in statistically significant increase in cell spreading, illustrated by increased average cell area (Figure 2K). Measured cell area increased from 950 μm^2 for A673 Ewing sarcoma cells harboring empty vector to >1500 μm^2 for cells expressing one or more of the adhesion proteins (Figure 2K). Consistent with the findings with A673 cells, expression of zyxin and α5 integrin, alone or in combination, was also sufficient to enhance cell area of EWS502 Ewing sarcoma cells, and enhanced actin cytoskeletons and focal adhesions were prominently induced by expression of zyxin (Supplemental Figure S1). Reexpression of zyxin induced a more robust spreading response than what occurred with reexpression of α5 integrin, although both displayed more extensive cell spreading than the parental A673 Ewing sarcoma cells. Of interest, Ewing sarcoma cells programmed to knock down EWS/FLI displayed an average cell area (~2200 μm^2) that was indistinguishable from the average area of cells expressing either zyxin alone or in combination with α5 integrin, illustrating that reexpression of zyxin is sufficient to fully rescue the cell spreading deficit observed in Ewing sarcoma cells.

The increased cell spreading and focal adhesion assembly was associated with enhanced adhesion, as measured in a quantitative, short–time course cell adhesion assay (Figure 2L). In this 2-h adhesion assay, the cells were allowed to adhere to an uncoated plastic tissue culture dish. Knockdown of EWS/FLI expression resulted in a statistically significant increase in cell adhesion (Figure 2L). Reexpression of α5 integrin alone or with zyxin enhanced cellular adhesion comparable to cells in which EWS/FLI expression was knocked down by RNAi. Although Ewing sarcoma cells reexpressing zyxin also displayed increased cell adhesion by this assay, the effect was not as dramatic as in the case of α5 integrin expression (Figure 2L). The profound yet differential capacities of zyxin and α5 integrin to restore cell spreading, actin cytoskeleton, and focal adhesion number are summarized schematically in Figure 2M.

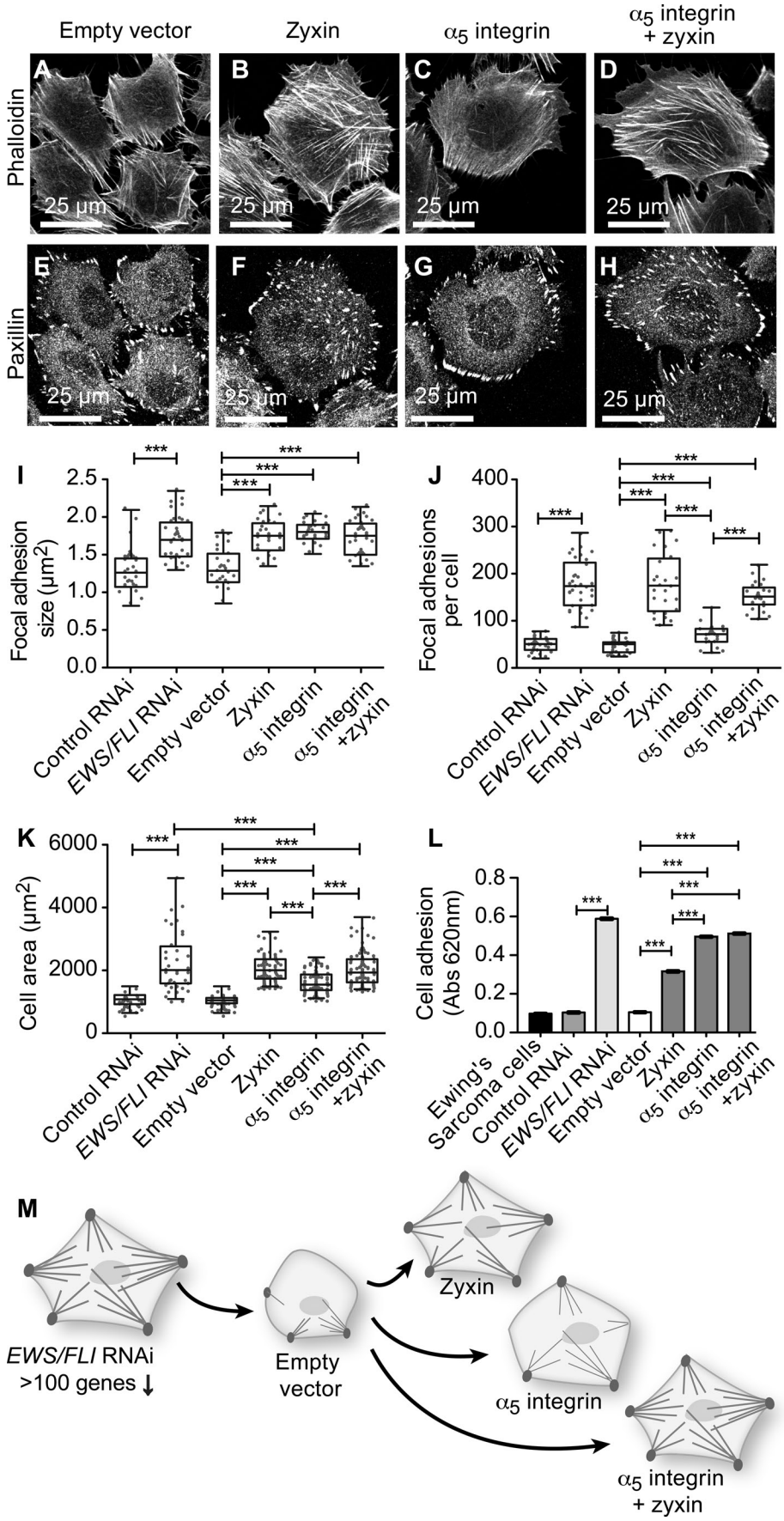

Intratibial orthotopic mouse model for Ewing sarcoma recapitulates features of the human disease

The ultimate goal of our studies was to understand the critical cellular mechanisms that are compromised in EWS/FLI-transformed cells and decipher the consequences of these alterations for tumor biology. To test whether increasing cellular adhesion by the reexpression of zyxin and α5 integrin in Ewing sarcoma cells would affect tumor cell

FIGURE 2: Zyxin and α5 integrin contribute to the actin cytoskeleton, focal adhesions, cell spreading, and cell adhesion in Ewing sarcoma cells. (A–H) A673 cells engineered to express empty vector (A, E), zyxin (B, F), α5 integrin (C, G), or both α5 integrin and zyxin (D, H) were stained for actin filaments (phalloidin, A–D) and focal adhesions (paxillin, E–H), followed by immunofluorescence microscopy. Control A673 cells were small and round, with minimal actin stress fibers and few focal adhesions. Cells that express zyxin, α5 integrin, or both α5 integrin and zyxin were well spread, with prominent focal adhesions. Focal adhesion size (I) and number per cell (J) were quantitated for at least 25 cells (each condition) and compared between control and EWS/FLI RNAi cells and cells that express zyxin, α5 integrin, or both α5 integrin and zyxin. (K) Total cell area was measured in at least 35 phalloidin-stained cells with either RNAi (control and EWS/FLI) or with expression of zyxin, α5 integrin, or both α5 integrin plus zyxin. Cell spreading and area increased with EWS/FLI knockdown and with expression of zyxin and α5 integrin. (L) Cell adhesion was evaluated by plating cells for 2 h, followed by colorimetric detection. Data are graphed as mean with SEM (six wells each cell type). Cells with control RNAi or empty vector adhered less than cells with EWS/FLI RNAi or cells that express zyxin, α5 integrin, or both α5 integrin and zyxin. (M) Model of Ewing sarcoma cell phenotypes. The actin cytoskeleton and focal adhesions, cell spreading, and cell area are changed by these proteins in unique and distinct ways. EWS/FLI expression compromises Ewing sarcoma cell adhesion by influencing actin cytoskeleton, cell morphology, and spreading, perhaps due to the down-regulation of cell adhesion proteins in general and of zyxin and α5 integrin in particular. For I–K, data are graphed as box-and-whisker plot (median with 25% quartile above and below in the box, and whiskers as minimum to maximum), with the individual data points included as scatter plot. Bars identify the data sets compared in parametric unpaired *t* tests. ***$p < 0.001$; other comparisons were not statistically different.

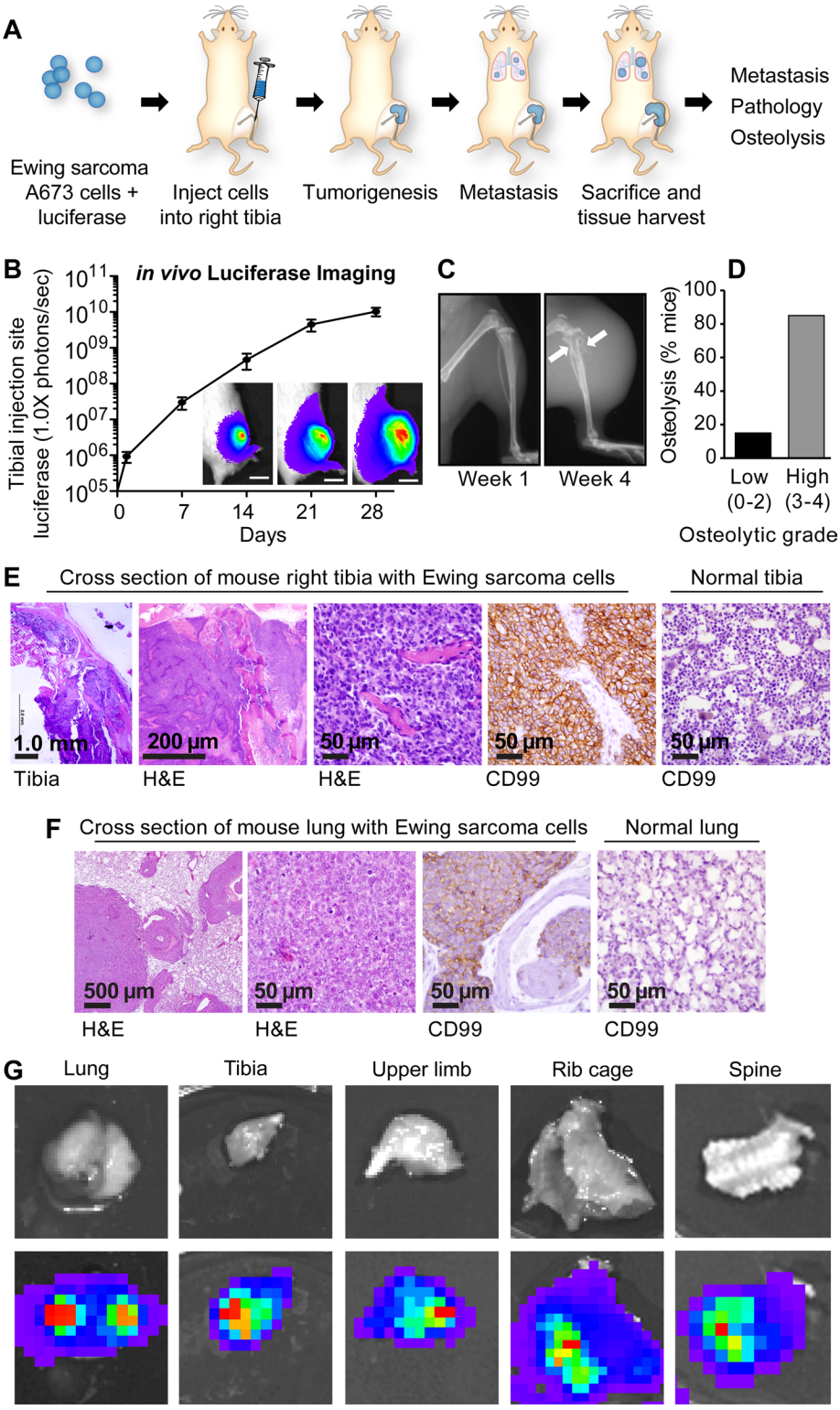

FIGURE 3: Intratibial orthotopic mouse model for Ewing sarcoma recapitulates features of the human disease. (A) Schematic diagram of the orthotopic mouse model, in which A673 Ewing sarcoma cells engineered to express luciferase were injected into the tibia, then monitored weekly for 4 wk for tumor growth, osteolysis, and metastasis, followed by ex vivo analysis and histopathology. (B) Tibial tumor growth and proliferation of Ewing sarcoma cells were measured by in vivo luciferase bioluminescence imaging. Data are graphed as mean with SEM, $n = 5$ mice. (C) Osteolysis (white arrows indicate regions of bone loss) increased compared with the same mouse tibia at week 1. (D) Qualitative analysis of mouse radiographs by an independent analyst revealed ~85% of mice had high-grade osteolysis (grade 3 or 4) in the injected tibias. (E) Histopathological analysis of tibial tumors showed highly invasive tumor in the tibia (1, 5×) and closer examination (2, 20×; and 3, 400×) revealed the presence of typical small, round, blue Ewing sarcoma cells. Membranous staining for Ewing sarcoma marker CD99 (brown staining in 4) confirmed Ewing sarcoma cells in the tibial tumor, and CD99 staining was negative in a normal tibia (5). (F) Mouse lung with metastatic lesions sectioned and stained by H&E (1, 2) also contained small, round, blue cells typical of Ewing sarcoma, and the lung was positive for Ewing sarcoma marker CD99 (brown staining in 3) and negative for CD99 in a normal lung (4). (G) Representative ex vivo luciferase imaging to evaluate metastasis in lungs and bones at harvest.

behavior in vivo, we first established an orthotopic xenograft model in our lab that faithfully replicates key aspects of Ewing sarcoma behavior. Xenograft models of Ewing sarcoma cells implanted at nonorthotopic sites in mice (e.g., subcutaneous flank injections in nude mice) are useful for evaluating tumor growth response to cell type or drug treatment (Smith *et al.*, 2006; Houghton *et al.*, 2010; Sankar *et al.*, 2013b; Ambati *et al.*, 2014), but such models do not account for the complexity of the bone microenvironment for either primary tumor establishment or metastasis to secondary sites. Studies in which Ewing sarcoma cells have been introduced directly into mouse tibias have enabled examination of tumor-induced osteolytic bone destruction and dissemination from the orthotopic site (Guan *et al.*, 2008; Hauer *et al.*, 2013). Luciferase tagging of Ewing sarcoma cells before orthotopic injection enables in vivo bioluminescence imaging to track tumor cell location (Wang *et al.*, 2009). Building on these prior approaches, we injected luciferase-expressing A673 Ewing sarcoma cells that were suspended in Matrigel into tibias of immunodeficient mice. After tumor cell introduction, we systematically monitored tumor growth and progression, osteolysis, and metastasis (Figure 3A).

Under our experimental conditions, tumors grew rapidly and were highly osteolytic. Most of the mice (14 of 15) formed tumors in the injected tibia that were palpable and measurable by in vivo luciferase imaging, and we observed aggressive growth of these tumors (Figure 3B). Tibial radiographs revealed extensive osteolysis (Figure 3C), a common characteristic of Ewing sarcoma progression in human patients. Radiographic analysis revealed that 85% of mice displayed cortical bone destruction and massive bone loss by week 4, warranting a classification of grade 3 or 4 osteolysis (Figure 3D).

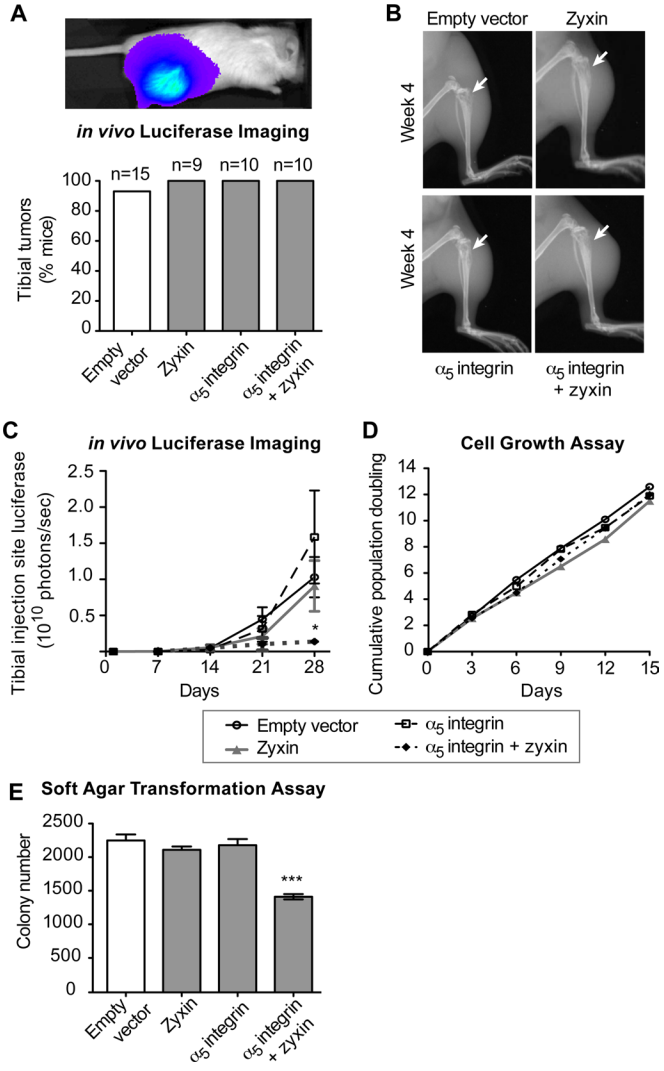

FIGURE 4: Zyxin and α5 integrin coexpression in Ewing sarcoma cells reduce tumor growth, whereas osteolytic degradation of bone persists. (A) In vivo luciferase imaging of mice 4 wk after intratibial injections with Ewing sarcoma A673 cells engineered to express empty vector, zyxin, α5 integrin, or both α5 integrin and zyxin. Every cell type was capable of inducing tibial tumors detectable by bioluminescence imaging. (B) Radiographs of tibias 4 wk after injections with cells that express empty vector, zyxin, α5 integrin, or both α5 integrin and zyxin revealed high-grade osteolysis (white arrows) regardless of which cell type was injected. (C) In vivo luciferase imaging of tibial tumors for 4 wk. Bioluminescence signals restricted to the tibial tumor region were quantitated (photons/second) and graphed over time as mean with SEM. *$p < 0.05$ for unpaired *t* test between empty vector group ($n = 15$ mice) and α5 integrin plus zyxin group ($n = 10$ mice). Expression of α5 integrin plus zyxin in Ewing sarcoma cells inhibited the tumor growth compared with the other groups. (D) 3T5 cell growth assay of A673 Ewing sarcoma cells with empty vector, zyxin, α5 integrin, or both α5 integrin and zyxin did not detect a difference in growth and proliferation in culture. Data from a single experiment are shown, representative of three sets of cell growth assays. (E) Soft-agar transformation and colony formation of cells with empty vector, zyxin, or α5 integrin alone were not different. However, colony formation in soft agar was inhibited in A673 cells that expressed both α5 integrin and zyxin. Graph is shown as mean with SEM, and ***$p < 0.001$ in unpaired Student's *t* test between empty vector and α5 integrin plus zyxin data sets.

Ewing sarcoma is distinguished by its small, round, blue cell morphology when tissue biopsy sections are stained with hematoxylin and eosin (H&E), as well as by distinct membrane labeling with antibodies directed against CD99, a transmembrane glycoprotein that serves as a diagnostic biomarker for Ewing sarcoma (Ambros *et al.*, 1991; Fellinger *et al.*, 1991; Perlman *et al.*, 1994). Consistent with features observed in clinical samples, the histological presentation and positive CD99 staining of Ewing sarcoma cells in the mouse model were indistinguishable from what is observed in human patient samples (Figure 3E), illustrating preservation of key morphological properties of the human tumor cells in the context of the murine host. The CD99 staining further confirmed the human origin of the cells, since mice do not express this marker.

In patients, Ewing sarcoma arises in bone and has a propensity to metastasize to lung and other bones (Arndt and Crist, 1999; Spraker *et al.*, 2012). This metastatic profile is also preserved in our orthotopic xenograft model (Figure 3, F and G). In vivo imaging of the luciferase-tagged Ewing sarcoma cells in the mice revealed that half exhibited positive signal in the chest area, suggesting potential metastasis to the lungs. On dissection and histopathological analysis, lungs that were luciferase positive exhibited small, round, blue cells by H&E staining and positive anti-CD99 labeling, confirming the presence of metastatic Ewing sarcoma cells (Figure 3F). Luciferase imaging of the mouse carcass revealed metastasis to other sites, such as the left tibia or upper limb and occasionally ribs and spine (Figure 3G). Establishment of a robust mouse model system for Ewing sarcoma that recapitulates key clinical features of the human disease set the stage for studies of the effect of EWS/FLI dependent gene regulation in vivo.

EWS/FLI-dependent repression of zyxin and α5 integrin expression enhances anchorage-independent growth of Ewing sarcoma cells

To probe the effect of EWS/FLI-dependent repression of zyxin and α5 integrin expression, we introduced Ewing sarcoma cells that were engineered to reexpress one or both of these proteins into recipient mice via intratibial injection, as described, and compared the growth of the resulting primary tumors with those derived from parental A673 cells. In all four groups (A673 parental, zyxin reexpression, α5 integrin reexpression, and zyxin plus α5 integrin reexpression), 90–100% of the mice formed luciferase-positive tumors within 4 wk after intratibial injection (Figure 4A). Histological analysis of tissue sections taken at week 4 revealed that all of the tumors exhibit small, round, blue cell morphology characteristic of Ewing sarcoma and were CD99 positive by immunohistochemistry (Supplemental Figure S2). Light microscopic examination revealed no differences among the four tumor groups. Similarly, significant osteolysis (>grade 3) was evident in radiographs of the affected tibias at 4 wk for tumors derived from all four cell variants (Figure 4B).

Although all four tumor cell variants formed palpable tumors and osteolytic lesions, in vivo luciferase-based imaging of tumors derived from A673 cells coexpressing zyxin and α5 integrin revealed slower tumor growth than tumors derived from either parental A673 cells or cells expressing just one of the transgenes (Figure 4C). This observation suggests that EWS/FLI-mediated down-regulation of zyxin and α5 integrin synergistically facilitates tumor growth.

The reduction in primary tumor growth by Ewing sarcoma cells that expressed both zyxin and α5 integrin raised the possibility that reexpression of these two focal adhesion proteins might affect cell proliferation rate. To test this possibility directly, we measured cell growth in culture (Figure 4D). The three reexpression lines displayed growth curves that were indistinguishable from that of the parental

A673 Ewing sarcoma cells, indicating that anchorage-dependent cell proliferation was not detectably influenced by altering zyxin or α5 integrin levels. In striking contrast, simultaneous reexpression of zyxin and α5 integrin in A673 cells results in ~40% reduction in the number of cell colonies in a soft-agar transformation assay, whereas neither individual protein had a statistically significant effect (Figure 4E). Consistent with our quantitative analysis of viable tumor cells by in vivo luciferase monitoring in Figure 4C, coexpression of zyxin and α5 integrin synergistically retards cell growth in soft agar. Thus the reduction in zyxin and α5 integrin that occurs in response to EWS/FLI expression appears to enhance the cells' capacity to grow under anchorage-independent conditions.

EWS/FLI-dependent repression of α5 integrin expression abrogates metastatic lung colonization

Because of the effect of cell adhesion in establishing metastatic potential (Arjonen *et al.*, 2011; Patel *et al.*, 2011), it was of interest to evaluate whether repression of zyxin and/or α5 integrin expression influences this process. The tibial injection model we developed, in which metastasis of Ewing sarcoma cells follows the pattern of sites observed clinically in patients, enabled us to probe the roles of zyxin and/or α5 integrin in the spatial and temporal regulation of metastasis. A673 parental Ewing sarcoma cells or cells engineered to reexpress zyxin and/or α5 integrin were introduced into recipient mice by intratibial injection and were followed by weekly in vivo luciferase imaging for 4 wk to evaluate the rate at which metastasis (positive chest signal) developed for each A673 sarcoma cell variant (Figure 5A). By 14 d after intratibial injection, intravital imaging revealed evidence of tumor burden beyond the initial site of tumor cell injection in all sample groups; however differential levels of metastasis were already evident for the different molecular variants of A673 Ewing sarcoma cells. A higher percentage of the mice injected with Ewing sarcoma cells that reexpressed α5 integrin alone or in concert with zyxin displayed positive luciferase signal in the chest earlier than mice injected with Ewing sarcoma cells harboring empty vector (Figure 5A). By week 4 (Figure 5B), metastasis was evident by in vivo imaging in 90–100% of the animals injected with A673 sarcoma cells that reexpressed α5 integrin alone or with zyxin. In contrast, only 56% of animals injected with A673 cells programmed to reexpress zyxin and 47% of animals injected with parental A673 cells exhibited chest signal at week 4 (Figure 5B).

We further examined the metastatic profile of the Ewing sarcoma tumor variants by macroscopic examination of organs isolated by dissection followed by histological staining and immunohistochemistry. The majority of dissected lungs had macroscopically visible metastatic lesions. Lungs derived from mice injected with cells expressing α5 integrin either alone or with zyxin were extensively riddled with lesions at an elevated frequency (Figure 5C). Stained sections of lung tissue displayed small, round, blue cells that were positive for the Ewing sarcoma marker CD99 (Figure 5C). When dissected bones and organs of mice were examined for presence of metastasis by luciferase imaging, mice across all four groups showed presence of bone metastasis in addition to lung metastasis (Figure 5D). Common sites for presence of bone metastasis were uninjected leg, upper limb, spine, and ribs, recapitulating what occurs in human patients.

Reexpression of adhesion proteins in Ewing sarcoma cells increases the cellular adherence to lung parenchyma in vivo

To test whether the increased adhesion of Ewing sarcoma cells reexpressing zyxin and/or α5 integrin could explain the enhanced incidence of detectable metastatic lung lesions in our mouse experiments, we used a competitive lung colonization assay in which we differentially labeled Ewing sarcoma cells harboring empty vector using the red lipophilic dye DiI and cells reexpressing zyxin and/or α5 integrin green using the lipophilic dye DiO. An equal mix of control cells and cells reexpressing zyxin and/or α5 integrin was introduced into the bloodstream of immunodeficient mice via tail-vein injection (Padua *et al.*, 2008; Chaturvedi *et al.*, 2012). Lungs were harvested 24 h postinjection and cryosectioned. We scanned 15 such representative sections measuring 4 mm^2 in area for the presence of fluorescently labeled red or green cells adhering to lung parenchyma, using confocal microscopy (Figure 6, A–C). Some tumor cells were present within capillaries, whereas others appeared to have extravasated out of the capillary bed. Although Ewing sarcoma cells adhered to the lung tissue, we observed an elevated number of tumor cells in the lungs when zyxin and/or α5 integrin were reexpressed. This was clearly indicated by increased number of green cell colonies in the lung parenchyma sections compared with red cell colonies (Figure 6). Expression of zyxin (Figure 6A), α5 integrin (Figure 6B), or both zyxin and α5 integrin (Figure 6C) significantly increased the number of tumor cells resident in the lung (Figure 6D). As discussed later, although an increased tumor cell burden was clearly evident in the lungs when the tumor cells were programmed to express zyxin and/or α5 integrin, it is not clear whether this is due to increased dwell time within the capillaries, improved adhesion to target lung parenchyma, or both.

DISCUSSION

Nearly all cases of Ewing sarcoma harbor the t(11;22) chromosomal translocation and are aggressive and micrometastatic at presentation. However very little is understood about how EWS/FLI expression, which represses many more genes than it activates, affects complex cell behaviors that dictate Ewing sarcoma tumor progression and metastasis (May *et al.*, 1993b; Smith *et al.*, 2006; Owen *et al.*, 2008). Our recent work (Chaturvedi *et al.*, 2012) established that EWS/FLI expression triggers a profound loss of cell adhesion and disturbance of actin cytoskeletal architecture. To dissect the mechanism by which EWS/FLI induces these tumor cell properties, we used patient-derived Ewing sarcoma cell lines to identify the misregulated genes responsible for the tumor phenotypes. This study links specific genes that are misregulated by EWS/FLI expression to the phenotypic alterations in cytoskeletal integrity and adhesiveness observed in patient-derived Ewing sarcoma cells.

Consistent with our findings that knockdown of EWS/FLI expression in Ewing sarcoma cells results in a dramatic alteration in cell adhesion and cytoarchitecture, analysis of the gene expression signature of EWS/FLI using a previously published microarray (Owen *et al.*, 2008) revealed that the most prominent down-regulated targets of EWS/FLI were focal adhesion proteins, ECM–receptor proteins, and regulators of the actin cytoskeleton. This collection of EWS/FLI-repressed genes could play a critical role in modulating tumor cell adhesion, cell spreading, and interaction of tumor cells with their environment to influence tumor progression and metastasis. Here we dissected the effect of two such EWS/FLI down-regulated targets, zyxin (a focal adhesion protein) and α5 integrin, which, along with the β1 integrin subunit, forms the receptor for binding fibronectin, a prominent bone matrix component. We reexpressed these proteins in patient-derived Ewing sarcoma cells either alone or in combination with each other to identify the unique and distinct contributions of zyxin and α5 integrin in Ewing sarcoma biology, both in vitro and in vivo. The reexpression of α5 integrin and zyxin within Ewing sarcoma cells results in a striking morphological change in the sarcoma cells that is essentially indistinguishable from what

occurs when the expression of the transforming oncogene itself is compromised by RNAi (Chaturvedi *et al.*, 2012). Thus our findings identify central aspects of the mechanism by which morphological transformation is achieved by the EWS/FLI oncogene.

Reexpression of α5 integrin in the small, round Ewing sarcoma cells enhances cell adhesion as measured in a short-term (2-h) quantitative cell adhesion assay. Expression of α5 integrin results in a statistically significant increase in focal adhesion size relative to control cells, as well as enhanced cell spreading as assayed by cell area measurements, and correlates morphological changes with the elevated retention of cells when plated on fibronectin. Expression of

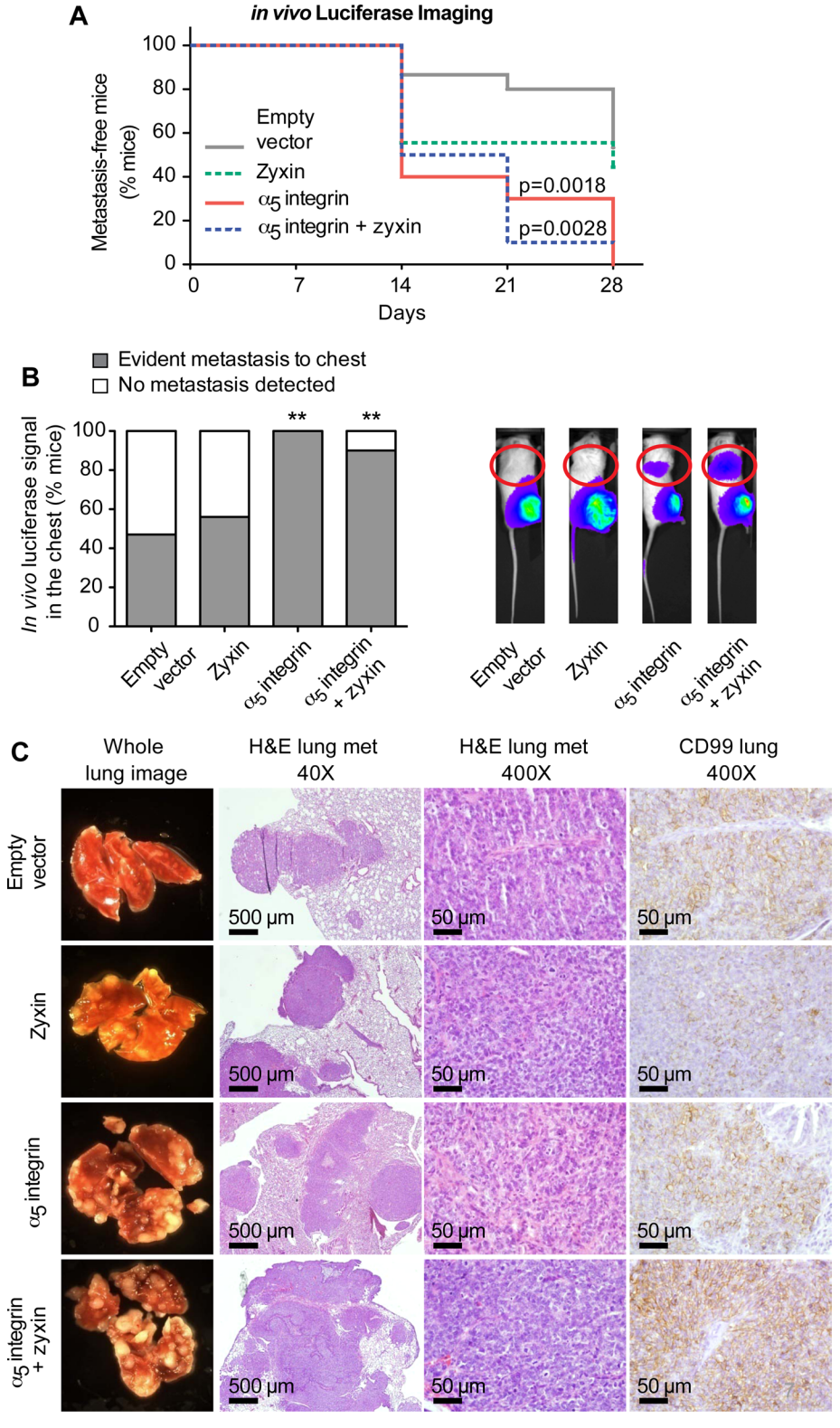

D

ex vivo luciferase imaging of the dissected animal	Empty vector	Zyxin	α5 integrin	α5 integrin + zyxin
	Number of mice / Total mice (%)			
Bones (uninjected tibia, upper limbs, rib-cage, spine)	11/15 (73%)	5/9 (56%)	7/10 (70%)	6/10 (60%)
Lungs	7/15 (47%)	4/9 (44%)	7/10 (70%)	9/10 (90%)

FIGURE 5: Ewing sarcoma cells that express zyxin and α5 integrin metastasize to lungs and bones. (A) Metastasis-free survival curve of mice evaluated by in vivo luciferase imaging of the four cell-type groups at weekly intervals. Metastasis was defined as appearance of bioluminescence signal other than at injection site, primarily the chest area. In unpaired *t* tests between the empty vector group and the α5 integrin group, $p = 0.0018$, and between the empty vector group and the α5 integrin plus zyxin group, $p = 0.0028$. (B) Week 4 endpoint images of in vivo luciferase signal were examined for metastasis. Almost all mice injected with Ewing sarcoma cells that expressed α5 integrin, either alone or in combination with zyxin, had significant metastasis by in vivo imaging, whereas only half the mice injected with empty vector control cells or with zyxin-expressing cells had in vivo chest signal at 4 wk. Dissection of the mice revealed the chest signals were due to heavy involvement of lungs. $^{**}p < 0.01$ in unpaired Student's *t* tests between empty vector group and α5 integrin alone or α5 integrin plus zyxin group. (C) Lungs exhibited macroscopically visible lesions (1) that were obvious in every mouse. Paraffin-embedded lungs were sectioned, and H&E staining identified multiple metastases characterized by the presence of small, round, blue cells (2, 3). Immunohistochemistry for the Ewing sarcoma marker CD99 on lung sections (4, brown signal) confirmed the presence of Ewing sarcoma cells. (D) Immediately after dissection, ex vivo luciferase signals of multiple organs and skeletal regions were examined for each mouse. The number of mice positive for luciferase signal in bones, lungs, or other organs was scored, and results are presented as percentage of mice in each group. For all groups of mice, the preferred metastatic sites were bones and lungs.

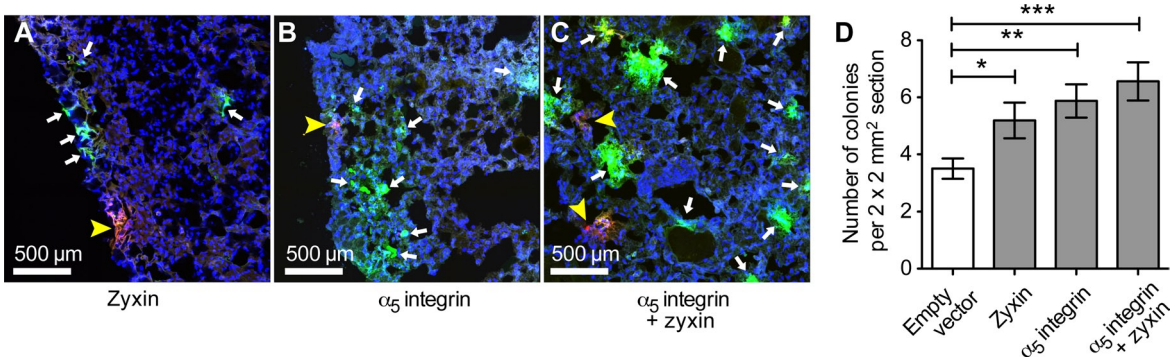

FIGURE 6: Ewing sarcoma cells that express zyxin and α5 integrin exhibit increased adhesion to lung parenchyma. In vivo lung adhesion assay of Ewing sarcoma cells that express empty vector (labeled red, DiI) and cells that express zyxin, α5 integrin, or both α5 integrin and zyxin (labeled green, DiO). Red and green cells were combined 1:1, and 1 million cells were injected into the tail veins of three mice and given 24 h to circulate and adhere. At 24 h, lungs were harvested, fixed, and cryosectioned. The numbers of red cell colonies and green cell colonies were evaluated by confocal microscopy of lung sections. (A–C) Maximum intensity projection of representative confocal images of lung sections, showing red cell colonies (empty vector, yellow arrowheads) vs. green cell colonies (expressing zyxin and/or α5 integrin, white block arrows) for all groups of mice. Nuclei are stained blue using DAPI. (D) Cell colonies were counted for 15 representative sections 4 mm^2 in area. Cells expressing zyxin or α5 integrin accumulated more in the lung parenchyma compared with empty vector control cells. In addition, cells expressing both zyxin and α5 integrin were the most adherent group of cells, with high affinity for lung parenchyma. Graph shows the mean with error bars for SEM. Bars identify the data sets compared in unpaired Student's *t* tests; *$p < 0.05$, **$p < 0.01$, ***$p < 0.001$.

α5β1 integrin has been shown to promote the acquisition of fibroblast-like cell morphology (Truong and Danen, 2009), consistent with our findings that the loss of integrin expression appears to play a key role in the loss of mesenchymal phenotype that accompanies EWS/FLI-dependent transformation (Chaturvedi *et al.*, 2012). Of interest, expression of α5 integrin did not lead to detectable improvement in actin cytoarchitecture and stress fiber integrity, illustrating the capacity of integrins to influence cell adhesion even when actin cytoarchitecture remains compromised by transformation.

In striking contrast to what is observed when α5 integrin expression is restored in Ewing sarcoma cells, the reexpression of zyxin results in a potent enhancement of actin stress fibers. The morphological changes induced in Ewing sarcoma cells by reintroduction of a single expression construct highlights zyxin as a master regulator of actin cytoarchitecture in these cells. We previously demonstrated that zyxin plays a central role in stabilizing and reinforcing actin stress fibers in response to mechanical stimulation (Yoshigi *et al.*, 2005; Smith *et al.*, 2010). Analysis of fibroblasts derived from mice in which the *zyxin* gene was disrupted revealed that spontaneous, strain-induced actin stress fiber breakage occurred with increased frequency (Smith *et al.*, 2010). The actin cytoskeletal deficit in Ewing sarcoma cells may therefore result from EWS/FLI-induced repression of zyxin expression that results in failure of the cytoskeletal repair machinery and unmitigated actin damage in the face of mechanical stress. The ability to restore cytoarchitecture by simple expression of zyxin also illustrates that core elements of the actin assembly machinery remain intact in Ewing sarcoma cells.

Reexpression of zyxin in Ewing sarcoma cells also leads to a significant increase in the number and size of focal adhesions, highlighting the previously described link between actin integrity and focal adhesion stability and maturation (Chaturvedi *et al.*, 2012). Our quantitative analyses revealed that α5 integrin and zyxin expression independently influence focal adhesion number/morphology and cell adhesion as monitored in a cell plating assay. However, the effects are not simply additive, with zyxin appearing to be the dominant player in the focal adhesion phenotype and α5 integrin serving as the dominant influence on cell adhesion.

The development of a high-fidelity orthotopic xenograft model for the study of Ewing sarcoma enabled us to explore the influence of zyxin and α5 integrin on tumor behavior in vivo. We initially expected the repression of zyxin and α5 integrin expression that occurs in Ewing sarcoma to provide a consistent "advantage" to the tumor cells throughout the tumor's life history. In accord with that view, we found that parental Ewing sarcoma cells with reduced zyxin and α5 integrin showed a growth advantage in vivo. In contrast with that view, the reduced expression of these two genes adversely affected second-site lung colonization. These contrasting effects on the overall "fitness" of the Ewing sarcoma cells at different stages in tumor progression provide an example of the kinds of tradeoffs that tumor cells make in their evolution (Bernards and Weinberg, 2002).

Exploring these tradeoffs in greater detail, analysis of parental Ewing sarcoma cells compared with cells reconstituted with zyxin and α5 integrin revealed that the reduction of zyxin and α5 integrin expression that occurs in Ewing sarcoma cells synergistically promotes intratibial tumor expansion in vivo, based on the use of bioluminescence imaging as a surrogate means of assessing tumor growth. This growth advantage was not recapitulated when cells were grown under two-dimensional culture conditions but was observed in vitro in a soft-agar cloning assay that reflects anchorage-independent cell growth potential. Of interest, hypoxia has been shown to induce upregulation of EWS/FLI expression and a similar enhancement of anchorage-independent, but not anchorage-dependent, Ewing sarcoma cell proliferation (Aryee *et al.*, 2010). The results presented here raise the possibility that at least part of the effect of hypoxia on Ewing sarcoma growth potential may be attributable to enhanced EWS/FLI-dependent repression of zyxin and α5 integrin expression.

Successful growth in soft agar reflects a tumor cell's resistance to anoikis, a form of detachment-induced cell death that limits the ability of normal cells to survive and grow in an inappropriate environment (Guadamillas *et al.*, 2011; Kim *et al.*, 2012). Integrin-dependent signaling influences anoikis in multiple ways. Whereas integrin

engagement is normally associated with promoting cell survival, unligated integrins have been shown to induce cell death via mechanisms involving recruitment and activation of specific caspases (Stupack *et al.*, 2001; Rajeswari and Pande, 2006). Fibronectin expression is repressed in Ewing sarcoma cells, and thus a corresponding reduction in α5 integrin expression would be predicted to reduce anoikis induced by unligated integrins, facilitating anchorage-independent cell growth. Although not yet linked mechanistically to integrin signaling and anoikis, zyxin was identified as a key intracellular mediator of apoptosis induced by antibody ligation of the Ewing sarcoma marker cell surface protein CD99 (Cerisano *et al.*, 2004). Zyxin has also been shown to interact directly with the cell cycle and apoptosis regulatory protein CARP-1 (Hervy *et al.*, 2010), providing further support for a role for zyxin in apoptotic signaling. The coordinated repression of zyxin and α5 integrin by EWS/FLI could thus promote survival of Ewing sarcoma cells while simultaneously enabling their release from the bone matrix, potentially promoting tumor cell dissemination from the primary site (Chaturvedi *et al.*, 2012).

In contrast with the growth and survival advantage achieved in Ewing sarcoma cells that is conferred by reduced expression of zyxin and α5 integrin, these changes in gene expression were associated with compromised ability of the tumors to metastasize to the lung. In this situation, the reduced levels of α5 integrin in Ewing sarcoma appeared to be primarily responsible for limiting lung metastasis compared with tumors in which α5 integrin expression was restored. A lung colonization assay in which parental Ewing sarcoma cells or cells reconstituted with zyxin and/or α5 integrin were introduced into the circulation by tail-vein injection revealed that the cells expressing the genes were more prominently observed in the lung parenchyma, indicating greater success in extravasation and/or adhesion at the second site. Consistent with our findings, a recent study of breast, kidney, and bladder tumor cells revealed that α5 integrin expression facilitates cancer cell adhesion and invasion (Mierke *et al.*, 2011). The ability of integrin to influence these properties was positively correlated with the tumor cells' ability to transmit and generate contractile forces.

Targeted therapies for Ewing sarcoma are not yet available clinically. Although evaluating the response of cultured Ewing sarcoma cells to a novel therapeutic agent is a common early step in drug development, the availability of robust animal models for the disease are essential to facilitate assessment of new agents. High-fidelity mouse models are only available for a limited number of cancer types. Many preclinical studies use xenografts in which human tumor cells are injected subcutaneously into immunocompromised mice. Although these ectopic xenograft models can be useful, they have numerous deficiencies, including the fact that the tumor cells do not reside in a microenvironment that is similar to what occurs in the patient, and the tumor models often behave very differently from what occurs in patients. To overcome this challenge, the development of orthotopic xenograft models that faithfully replicate the behavior of tumors in patients is a key priority. Recent advances in the development of orthotopic xenografts for breast cancer have revealed the power of preclinical models for predicting disease outcome (DeRose *et al.*, 2011; Lum *et al.*, 2012) and create powerful tools for preclinical testing of novel therapeutic interventions. Here we presented a method for the establishment of orthotopic xenograft models to study Ewing sarcoma. We observed that tumors seeded directly into a long bone of the mouse recapitulate osteolytic properties that occur in human patients and also metastasize to other bony sites in addition to lung. Tumor metastasis in our mouse model was not evident in liver or other vital organs, consistent with the metastatic profile observed in patients and highlighting the importance of tumor microenvironment (Kerbel, 1995; Mundy, 2002). Prior models established to study Ewing sarcoma metastasis typically involved direct inoculation of tumor cells into the vasculature by tail-vein injection (Scotlandi *et al.*, 2000; Hu-Lieskovan *et al.*, 2005). These models provide insights into the late aspects of metastatic progression, including extravasation and colonization at second sites. Bone injection approaches have been used to study Ewing sarcoma biology, including establishment, growth, and osteolytic properties in bone and secondary lung metastasis (Guan *et al.*, 2005, 2008; Wang *et al.*, 2009; Hauer *et al.*, 2013). We expanded on prior work to develop an orthotopic mouse model of Ewing sarcoma that shows spontaneous metastasis from the primary bony site to other bones within 4 wk. This intratibial model has been used effectively here and by our collaborators to investigate the contributions of Ewing sarcoma target genes on tumor growth and lung metastasis (Sankar *et al.*, 2013b; Wiles *et al.*, 2013). While our manuscript was being reviewed for publication, an intrafemoral model of luciferase-tagged Ewing sarcoma cells was reported as a system to study tumor cell dissemination to lung, liver/abdomen, and other bones, consistent with our findings (Vormoor *et al.*, 2014). The ability to manipulate the expression of specific genes in Ewing sarcoma cells and study their effect on tumor establishment and progression will allow a detailed mechanistic analysis of the roles of particular EWS/FLI targets for clinically relevant aspects of tumor biology. The preclinical mouse models for Ewing sarcoma that are now available should provide a powerful tool to assess mechanisms of tumor cell dissemination from the primary bony site and colonization at remote sites, as well as provide an improved preclinical environment for testing novel therapeutic agents.

MATERIALS AND METHODS

Reagents and antibodies

Antibodies were used for Western immunoblots, indirect immunofluorescence microscopy, and immunohistochemistry as per manufacturer's instructions: paxillin mouse antibody (P13520; Transduction Laboratories, San Jose, CA), FLI-1 rabbit antibody (15289; Abcam, Cambridge, MA), zyxin rabbit antibody (B71; Beckerle Lab), α5 integrin (610633; BD Bioscience, San Jose, CA), β-actin AC-74 mouse antibody and vinculin V9131 mouse antibody (Sigma-Aldrich, St. Louis, MO), α-tubulin mouse antibody (12G10; Developmental Studies Hybridoma Bank, Iowa City, IA), and CD99 (clone 0-13 mouse antibody; 620-01; Signet, Cambridge, UK). Secondary antibodies were horseradish peroxidase (HRP)–conjugated antibodies for immunoblots (GE Healthcare, Pittsburgh, PA), the Alexa Fluor antibodies and phalloidin for microscopy (Molecular Probes/Invitrogen, Grand Island, NY), and biotinylated rabbit anti-mouse antibody (E0413; Dako, Carpinteria, CA) for immunohistochemistry. Fibronectin to coat coverslips and Mowiol to mount coverslips (Sigma-Aldrich) and Vybrant Cell-Labeling solutions DiI and DiO (Molecular Probes/Invitrogen) were used as per manufacturer's instructions. D-Luciferin (Luck; Gold Biotech, St. Louis, MO) was injected for bioluminescence detection. Prolong Gold anti-fade reagent with 4′,6-diamidino-2-phenylindole (DAPI; P-36931; Invitrogen/Life Technologies) was used for mounting lung sections.

Cell culture

Ewing sarcoma cell lines A673 and EWS502 were grown in DMEM with 10% fetal bovine serum (FBS) and RPMI medium with 15% FBS, respectively, as previously published (Owen and Lessnick, 2006). Selection antibiotics used were puromycin (2 µg/ml; Sigma-Aldrich), neomycin (300 µg/ml; Life Technologies), and hygromycin (100 µg/ml; Invitrogen).

Constructs and retroviruses

Knockdown experiments used the luciferase-RNAi (as control RNAi) and EF-2-RNAi (as EWS/FLI RNAi) constructs in pSRP retroviral vector with a previously described puromycin resistance marker (Smith *et al.*, 2006; Chaturvedi *et al.*, 2012). For expression constructs, the human zyxin cDNA was cloned into pMSCV-neomycin retroviral vector (Clontech). The α5 integrin cDNA cloned in pMSCV-puromycin retroviral vector was a kind donation from Christopher Stipp (University of Iowa, Iowa City, IA). For luciferase expression in mice, pMMP-LucNeo or pMMP-LucHygro retrovirus was used as previously described (Owen and Lessnick, 2006). After retroviral infection for 2 d, cells were selected (puromycin, neomycin, or hygromycin) for 2 d before use and maintained for up to 5 wk.

Western blots

Whole-cell lysates in RIPA buffer (10 mM Tris-HCl, pH 7, 100 mM NaCl, 1 mM EDTA, 1% Triton X-100, 0.5% sodium deoxycholate, 0.1% SDS) with Complete Mini-EDTA-free protease inhibitor cocktail tablets (11836153001; Roche Diagnostics GmbH, Indianapolis, IN) were electrophoresed (15–30 μg/lane) on 10% SDS–PAGE gels and transferred onto nitrocellulose membranes. Proteins were detected with antibodies for FLI-1 (1:2000), zyxin (1:10,000), α5 integrin (1:5000), tubulin (1:10,000), vinculin (1:10,000), and HRP-conjugated secondary antibodies, followed by Enhanced ChemiLuminescence detection (GE Healthcare).

Immunofluorescence microscopy

The staining, microscopy, imaging, and analysis of fluorescently labeled cells were done as previously described (Chaturvedi *et al.*, 2012). A673 cells (75,000 cells) were plated on fibronectin-coated (10 μg/ml) coverslips in 12-well plates for 24 h, fixed in 3.7% formaldehyde for 15 min, and permeabilized in 0.2% Triton X-100/phosphate-buffered saline (PBS) for 5 min. Cells were incubated with paxillin antibody (1:100) for 1 h at 37°C, washed (PBS), stained with Alexa Fluor anti-mouse antibody (1:200), Alexa Fluor–phalloidin (1:100), and DAPI (1:600) for 1 h at 37°C, washed (PBS), and mounted in Mowiol medium. Cell images were captured with a Zeiss Axioskop2 mot plus microscope with a 40× objective (numerical aperture [NA] 0.75 NeoFluor), AxioCam MR camera, and AxioVision software, version 4.8.1 (Carl Zeiss MicroImaging), or with a Nikon A1R Ti inverted microscope, 60× oil objective (NA 1.4 Plan Apo DIC N2), and Nikon Elements software, version 3.

Cell area, number, and size of focal adhesions

These parameters in Ewing sarcoma cells stained with paxillin antibody and phalloidin were analyzed using immunofluorescence images (Nikon A1R Ti inverted microscope with 60× oil objective) as previously described (Chaturvedi *et al.*, 2012). Briefly, by use of the trace tool the boundaries of phalloidin-stained cells were outlined and area of the selected region measured (MetaMorph software, version 7.5; Molecular Devices, Sunnyvale, CA). To count and measure the size of the paxillin-rich focal adhesions, single-cell images were first processed (despeckle, remove noise, background subtraction with rolling ball) in ImageJ (National Institutes of Health, Bethesda, MD). Image threshold was set in single-cell images, and the area of the thresholded region represented the size of focal adhesions (MetaMorph, version 7.5). To measure focal adhesions using paxillin signal, at least 25 cells were measured per cell type. To measure cell area, at least 35 cells were measured per cell type.

3T5 cell growth assays

These assays were performed three times in duplicate as described in Smith *et al.* (2006). Briefly, 5×10^5 cells were seeded into 10-cm dishes for growth in tissue culture and counted every third day to determine the rate of cell proliferation and population doubling time.

Soft-agar transformation assays

These assays were performed in duplicate as previously described (Lessnick *et al.*, 2002; Chaturvedi *et al.*, 2012). In short, 1×10^5 cells were seeded in 0.35% agarose made in Iscove's modified Eagle's medium, penicillin/streptomycin, and glutamine with or without selection, grown for 3–4 wk, imaged, and colony count noted.

Adhesion assays

These assays were performed at least three times per cell type following previously published protocols (Hoffman *et al.*, 2006; Chaturvedi *et al.*, 2012). Ewing sarcoma cells (300,000) were seeded in triplicate onto a non–ECM coated 24-well plate for 2 h at 37°C, fixed in 3.7% formaldehyde (15 min), stained with 1% toluidene blue for 1 h, washed, air dried, and dissolved in 2% SDS. Optical density was measured at 620 nm.

In vivo mouse model

All animal protocols were approved by the Institutional Animal Care and Use Committee at the University of Utah. Male 5- to 6-wk-old NOD/SCID mice (strain code 394; Charles River Labs, Troy, NY) were obtained and housed at the University of Utah for 1 wk before experiments. The intratibial tumor injection studies were modified from a previously published method (Guan *et al.*, 2008). Mouse tibias were predrilled with a 26-g needle and x-rayed to validate needle placement; then luciferase-expressing Ewing sarcoma cells (2.5×10^5 cells in 10 μl of Matrigel), control A673 cells with empty vectors ($n = 15$ mice), and A673 cells engineered to express zyxin ($n = 9$ mice), α5 integrin ($n = 10$ mice), or both zyxin and α5 integrin together ($n = 10$ mice) were injected with a glass Hamilton syringe and 45° bevel 26-g needle. Tumor growth was monitored weekly for 4 wk by anesthetizing (isoflurane) the mice, injecting mice intraperitoneally with luciferin, and measuring the emitted photons per second (Xenogen IVIS 100 Imager and Living Image software, version 2.50.2; Perkin-Elmer, San Jose, CA). Tumor volume was measured with calipers and calculated using the formula $0.5a \times b \times c$, where a, b, and c are the three maximum diameters. Consistent with our animal protocol, mice were killed when tibial tumors measured 2 cm in width. Weekly x-rays were recorded (Kodak DXS4000), and osteolytic destruction of injected tibias was scored in a blind study by an independent analyst (R.L.R.). Bone lysis was graded on a scale of 0–4, where grade 0 represented no bone loss, grade 1 minimal but visible, grade 2 moderate (no cortex affected), grade 3 severe (cortex disrupted), and grade 4 massive bone destruction (Guan *et al.*, 2008). Before their harvest, mice received a final luciferin injection and were killed, the lungs were perfused intratracheally with 4% paraformaldehyde, and the bone tumors and lungs were removed, imaged for ex vivo luciferase signal, and fixed in neutral buffered Formalin. Ex vivo luciferase signal of organs (lung, liver, spleen, kidney, heart, testes, injected tibias, and uninjected bones) was used to evaluate other sites of metastasis. Before paraffin embedding, the fixed lungs were photographed (whole-lung images) to evaluate macroscopically visible lesions.

Immunohistochemical analysis

The fixed bone tumors were decalcified for 7 d before embedding in paraffin. The embedded tibias and lungs were sectioned and

stained with H&E, or IHC for CD99 (ARUP Laboratories, Salt Lake City, UT). The expression of CD99 was detected using clone O-13 anti-mouse antibody (1:200 dilution) for 2 h at 37°C. Biotinylated secondary antibody (1:100) was applied for 32 min at 37°C. Signals were detected with a streptavidin-HRP system, using 3-3′ diaminobenzidine as the chromogen (Research DAB Detection Kit; Ventana Medical Systems, Tucson, AZ). The slides were counterstained with hematoxylin (Ventana Medical Systems) for 8 min, gently washed in deionized H_2O/Dawn detergent mixture, placed in iodine for 30 s, then dipped in sodium thiosulfate, dehydrated in graded alcohols (70%, 95% ×2, and 100% ×2), and cleared in xylene; coverslips were then mounted (Sheryl Tripp at ARUP and Y.-C.L. at the Huntsman Cancer Institute). The tibia and lung sections were evaluated by an independent clinical pathologist (A.G.) in a blind study.

In vivo lung adhesion assay

This assay was done as previously described (Padua *et al.*, 2008; Chaturvedi *et al.* 2012). Briefly, A673 cells with empty vector were labeled with Vybrant DiI (red), and A673 cells with expression of zyxin, α5 integrin, or both zyxin and α5 integrin were labeled with Vybrant DiO (green). The red and green cells were mixed in a 1:1 ratio, and 1 million cells were injected into the tail vein of NOD/SCID mice (1303; Jackson Labs) and allowed 24 h to circulate in the mouse. Mice were killed after 24 h, and lungs were perfused intratracheally with 4% paraformaldehyde, removed, and cryopreserved in OTC freezing medium. Lungs were cryosectioned into 16-µm sections and examined on a Nikon A1R laser scanning confocal microscope (nine 2-µm optical sections, PlanFluor 40× oil DIC H N2 objective). A three field by three field (2 mm × 2 mm) mosaic image was created (NIS Elements software, version 3) and red versus green colonies counted in 15 representative fields from three mice. Two such biological replicates were done.

Microarray analysis

Previously published microarray data were reanalyzed for downregulated targets of EWS/FLI (Owen *et al.*, 2008). Expression data were filtered for a 1.8-fold change across samples, and significant changes were identified using permutation testing with a p of 0.01 after Benjamini and Hochberg correction and significant z-score in GeneSifter analysis software.

Statistical analysis

Statistical analysis and graphs were made using Prism 5 software (GraphPad, San Diego, CA). The box-and-whisker plots (median with 25% quartile above and below in the box; whiskers are minimum to maximum) and mean with SEM are given in the figure legends. The horizontal line above the graphs identifies the two groups compared using unpaired Student's t tests, which assumed a Gaussian distribution and equal SDs between populations. $p < 0.05$ in unpaired Student's t tests was considered significant. $^{*}p < 0.05$, $^{**}p < 0.01$, $^{***}p < 0.001$.

ACKNOWLEDGMENTS

We are grateful to Christopher Stipp for providing the pMSCVpuro-α5 integrin cDNA construct to overexpress α5 integrin. We thank Christopher Rodesch at the University of Utah Cell Imaging and Microscopy Core Facility for help with fluorescence imaging, image processing, and analysis, and we thank Brett Milash at the Huntsman Cancer Institute for help with microarray analysis. Ken Boucher of the Study Design and Biostatistics Shared Resource provided invaluable guidance with statistical analysis. Diana Lim provided expert help with figure design and preparation. This work was supported by the National Institutes of Health (R01 GM50877 to M.C.B. and R01 CA140394 to S.L.L.), the Huntsman Cancer Foundation, and the CureSearch for Children's Cancer Foundation. The Cancer Center Support Grant (2 P30 CA042014) awarded to the Huntsman Cancer Institute provided developmental funds and shared resources critical to this project.

REFERENCES

Ambati SR, Lopes EC, Kosugi K, Mony U, Zehir A, Shah SK, Taldone T, Moreira AL, Meyers PA, Chiosis G, *et al.* (2014). Pre-clinical efficacy of PU-H71, a novel HSP90 inhibitor, alone and in combination with bortezomib in Ewing sarcoma. Mol Oncol 8, 323–336.

Ambros IM, Ambros PF, Strehl S, Kovar H, Gadner H, Salzer-Kuntschik M (1991). MIC2 is a specific marker for Ewing's sarcoma and peripheral primitive neuroectodermal tumors. Evidence for a common histogenesis of Ewing's sarcoma and peripheral primitive neuroectodermal tumors from MIC2 expression and specific chromosome aberration. Cancer 67, 1886–1893.

Amsellem V, Kryszke MH, Hervy M, Subra F, Athman R, Leh H, Brachet-Ducos C, Auclair C (2005). The actin cytoskeleton-associated protein zyxin acts as a tumor suppressor in Ewing tumor cells. Exp Cell Res 304, 443–456.

Arjonen A, Kaukonen R, Ivaska J (2011). Filopodia and adhesion in cancer cell motility. Cell Adh Migr 5, 421–430.

Arndt CA, Crist WM (1999). Common musculoskeletal tumors of childhood and adolescence. N Engl J Med 341, 342–352.

Aryee DN, Niedan S, Kauer M, Schwentner R, Bennani-Baiti IM, Ban J, Muehlbacher K, Kreppel M, Walker RL, Meltzer P, *et al.* (2010). Hypoxia modulates EWS-FLI1 transcriptional signature and enhances the malignant properties of Ewing's sarcoma cells in vitro. Cancer Res 70, 4015–4023.

Aurias A, Rimbaut C, Buffe D, Zucker JM, Mazabraud A (1984). Translocation involving chromosome 22 in Ewing's sarcoma. A cytogenetic study of four fresh tumors. Cancer Genet Cytogenet 12, 21–25.

Bernards R, Weinberg RA (2002). A progression puzzle. Nature 418, 823.

Borinstein SC, Barkauskas DA, Krailo M, Scher D, Scher L, Schlottmann S, Kallakury B, Dickman PS, Pawel BR, West DC, *et al.* (2011). Investigation of the insulin-like growth factor-1 signaling pathway in localized Ewing sarcoma: a report from the Children's Oncology Group. Cancer 117, 4966–4976.

Braunreiter CL, Hancock JD, Coffin CM, Boucher KM, Lessnick SL (2006). Expression of EWS-ETS fusions in NIH3T3 cells reveals significant differences to Ewing's sarcoma. Cell Cycle 5, 2753–2759.

Campbell ID, Humphries MJ (2011). Integrin structure, activation, and interactions. Cold Spring Harb Perspect Biol 3, a004994.

Cavazzana AO, Miser JS, Jefferson J, Triche TJ (1987). Experimental evidence for a neural origin of Ewing's sarcoma of bone. Am J Pathol 127, 507–518.

Cerisano V, Aalto Y, Perdichizzi S, Bernard G, Manara MC, Benini S, Cenacchi G, Preda P, Lattanzi G, Nagy B, *et al.* (2004). Molecular mechanisms of CD99-induced caspase-independent cell death and cell-cell adhesion in Ewing's sarcoma cells: actin and zyxin as key intracellular mediators. Oncogene 23, 5664–5674.

Chaturvedi A, Hoffman LM, Welm AL, Lessnick SL, Beckerle MC (2012). The EWS/FLI Oncogene drives changes in cellular morphology, adhesion, and migration in Ewing sarcoma. Genes Cancer 3, 102–116.

Delattre O, Zucman J, Plougastel B, Desmaze C, Melot T, Peter M, Kovar H, Joubert I, de Jong P, Rouleau G, *et al.* (1992). Gene fusion with an ETS DNA-binding domain caused by chromosome translocation in human tumours. Nature 359, 162–165.

DeRose YS, Wang G, Lin YC, Bernard PS, Buys SS, Ebbert MT, Factor R, Matsen C, Milash BA, Nelson E, *et al.* (2011). Tumor grafts derived from women with breast cancer authentically reflect tumor pathology, growth, metastasis and disease outcomes. Nat Med 17, 1514–1520.

Ewing J (1921). Diffuse endothelioma of bone. Proc NY Pathol Soc 21, 17–24.

Fellinger EJ, Garin-Chesa P, Triche TJ, Huvos AG, Rettig WJ (1991). Immunohistochemical analysis of Ewing's sarcoma cell surface antigen p30/32MIC2. Am J Pathol 139, 317–325.

Geiger B, Yamada KM (2011). Molecular architecture and function of matrix adhesions. Cold Spring Harb Perspect Biol 3, a005033.

Guadamillas MC, Cerezo A, Del Pozo MA (2011). Overcoming anoikis—pathways to anchorage-independent growth in cancer. J Cell Sci 124, 3189–3197.

Guan H, Zhou Z, Gallick GE, Jia SF, Morales J, Sood AK, Corey SJ, Kleinerman ES (2008). Targeting Lyn inhibits tumor growth and metastasis in Ewing's sarcoma. Mol Cancer Ther 7, 1807–1816.
Guan H, Zhou Z, Wang H, Jia SF, Liu W, Kleinerman ES (2005). A small interfering RNA targeting vascular endothelial growth factor inhibits Ewing's sarcoma growth in a xenograft mouse model. Clin Cancer Res 11, 2662–2669.
Gupton SL, Riquelme D, Hughes-Alford SK, Tadros J, Rudina SS, Hynes RO, Lauffenburger D, Gertler FB (2012). Mena binds alpha5 integrin directly and modulates alpha5beta1 function. J Cell Biol 198, 657–676.
Hauer K, Calzada-Wack J, Steiger K, Grunewald TG, Baumhoer D, Plehm S, Buch T, Prazeres da Costa O, Esposito I, Burdach S, *et al*. (2013). DKK2 mediates osteolysis, invasiveness, and metastatic spread in Ewing sarcoma. Cancer Res 73, 967–977.
Herrero-Martin D, Osuna D, Ordonez JL, Sevillano V, Martins AS, Mackintosh C, Campos M, Madoz-Gurpide J, Otero-Motta AP, Caballero G, *et al*. (2009). Stable interference of EWS-FLI1 in an Ewing sarcoma cell line impairs IGF-1/IGF-1R signalling and reveals TOPK as a new target. Br J Cancer 101, 80–90.
Hervy M, Hoffman LM, Jensen CC, Smith M, Beckerle MC (2010). The LIM protein zyxin binds CARP-1 and promotes apoptosis. Genes Cancer 1, 506–515.
Hoffman LM, Jensen CC, Chaturvedi A, Yoshigi M, Beckerle MC (2012). Stretch-induced actin remodeling requires targeting of zyxin to stress fibers and recruitment of actin regulators. Mol Biol Cell 23, 1846–1859.
Hoffman LM, Jensen CC, Kloeker S, Wang CL, Yoshigi M, Beckerle MC (2006). Genetic ablation of zyxin causes Mena/VASP mislocalization, increased motility, and deficits in actin remodeling. J Cell Biol 172, 771–782.
Houghton PJ, Morton CL, Kang M, Reynolds CP, Billups CA, Favours E, Payne-Turner D, Tucker C, Smith MA (2010). Evaluation of cytarabine against Ewing sarcoma xenografts by the pediatric preclinical testing program. Pediatr Blood Cancer 55, 1224–1226.
Hu-Lieskovan S, Heidel JD, Bartlett DW, Davis ME, Triche TJ (2005). Sequence-specific knockdown of EWS-FLI1 by targeted, nonviral delivery of small interfering RNA inhibits tumor growth in a murine model of metastatic Ewing's sarcoma. Cancer Res 65, 8984–8992.
Hynes RO (2002). Integrins: bidirectional, allosteric signaling machines. Cell 110, 673–687.
Jedlicka P (2010). Ewing sarcoma, an enigmatic malignancy of likely progenitor cell origin, driven by transcription factor oncogenic fusions. Int J Clin Exp Pathol 3, 338–347.
Karosas AO (2010). Ewing's sarcoma. Am J Health Syst Pharm 67, 1599–1605.
Kerbel RS (1995). Significance of tumor-host interactions in cancer growth and metastases. Cancer Metastasis Rev 14, 259–262.
Kim YN, Koo KH, Sung JY, Yun UJ, Kim H (2012). Anoikis resistance: an essential prerequisite for tumor metastasis. Int J Cell Biol 2012 306879.
Kimber C, Michalski A, Spitz L, Pierro A (1998). Primitive neuroectodermal tumours: anatomic location, extent of surgery, and outcome. J Pediatr Surg 33, 39–41.
Kinsey M, Smith R, Lessnick SL (2006). NR0B1 is required for the oncogenic phenotype mediated by EWS/FLI in Ewing's sarcoma. Mol Cancer Res 4, 851–859.
Kovar H (2005). Context matters: the hen or egg problem in Ewing's sarcoma. Semin Cancer Biol 15, 189–196.
Lessnick SL, Braun BS, Denny CT, May WA (1995). Multiple domains mediate transformation by the Ewing's sarcoma EWS/FLI-1 fusion gene. Oncogene 10, 423–431.
Lessnick SL, Dacwag CS, Golub TR (2002). The Ewing's sarcoma oncoprotein EWS/FLI induces a p53-dependent growth arrest in primary human fibroblasts. Cancer Cell 1, 393–401.
Lotz MM, Rabinovitz I, Mercurio AM (2000). Intestinal restitution: progression of actin cytoskeleton rearrangements and integrin function in a model of epithelial wound healing. Am J Pathol 156, 985–996.
Lum DH, Matsen C, Welm AL, Welm BE (2012). Overview of human primary tumorgraft models: comparisons with traditional oncology preclinical models and the clinical relevance and utility of primary tumorgrafts in basic and translational oncology research. Curr Protoc Pharmacol 14, 14–22.
Margadant F, Chew LL, Hu X, Yu H, Bate N, Zhang X, Sheetz M (2011). Mechanotransduction in vivo by repeated talin stretch-relaxation events depends upon vinculin. PLoS Biol 9, e1001223.
Mateo-Lozano S, Tirado OM, Notario V (2003). Rapamycin induces the fusion-type independent downregulation of the EWS/FLI-1 proteins and inhibits Ewing's sarcoma cell proliferation. Oncogene 22, 9282–9287.
May WA, Gishizky ML, Lessnick SL, Lunsford LB, Lewis BC, Delattre O, Zucman J, Thomas G, Denny CT (1993a). Ewing sarcoma 11;22 translocation produces a chimeric transcription factor that requires the DNA-binding domain encoded by FLI1 for transformation. Proc Natl Acad Sci USA 90, 5752–5756.
May WA, Lessnick SL, Braun BS, Klemsz M, Lewis BC, Lunsford LB, Hromas R, Denny CT (1993b). The Ewing's sarcoma EWS/FLI-1 fusion gene encodes a more potent transcriptional activator and is a more powerful transforming gene than FLI-1. Mol Cell Biol 13, 7393–7398.
McAllister NR, Lessnick SL (2005). The potential for molecular therapeutic targets in Ewing's sarcoma. Curr Treat Options Oncol 6, 461–471.
Mierke CT, Frey B, Fellner M, Herrmann M, Fabry B (2011). Integrin alpha-5beta1 facilitates cancer cell invasion through enhanced contractile forces. J Cell Sci 124, 369–383.
Mostafavi-Pour Z, Askari JA, Parkinson SJ, Parker PJ, Ng TT, Humphries MJ (2003). Integrin-specific signaling pathways controlling focal adhesion formation and cell migration. J Cell Biol 161, 155–167.
Mundy GR (2002). Metastasis to bone: causes, consequences and therapeutic opportunities. Nat Rev Cancer 2, 584–593.
Nagae M, Re S, Mihara E, Nogi T, Sugita Y, Takagi J (2012). Crystal structure of alpha5beta1 integrin ectodomain: atomic details of the fibronectin receptor. J Cell Biol 197, 131–140.
Owen LA, Kowalewski AA, Lessnick SL (2008). EWS/FLI mediates transcriptional repression via NKX2.2 during oncogenic transformation in Ewing's sarcoma. PLoS One 3, e1965.
Owen LA, Lessnick SL (2006). Identification of target genes in their native cellular context: an analysis of EWS/FLI in Ewing's sarcoma. Cell Cycle 5, 2049–2053.
Padua D, Zhang XH, Wang Q, Nadal C, Gerald WL, Gomis RR, Massague J (2008). TGFbeta primes breast tumors for lung metastasis seeding through angiopoietin-like 4. Cell 133, 66–77.
Patel LR, Camacho DF, Shiozawa Y, Pienta KJ, Taichman RS (2011). Mechanisms of cancer cell metastasis to the bone: a multistep process. Future Oncol 7, 1285–1297.
Perlman EJ, Dickman PS, Askin FB, Grier HE, Miser JS, Link MP (1994). Ewing's sarcoma—routine diagnostic utilization of MIC2 analysis: a Pediatric Oncology Group/Children's Cancer Group Intergroup Study. Hum Pathol 25, 304–307.
Rajeswari J, Pande G (2006). Direct association between caspase 3 and alpha5beta1 integrin and its role during anoikis of rat fibroblasts. Cell Biol Int 30, 963–969.
Rodan SB, Rodan GA (1997). Integrin function in osteoclasts. J Endocrinol 154 (Suppl), S47–S56.
Salsmann A, Schaffner-Reckinger E, Kieffer N (2006). RGD, the Rho'd to cell spreading. Eur J Cell Biol 85, 249–254.
Sankar S, Bell R, Stephens B, Zhuo R, Sharma S, Bearss DJ, Lessnick SL (2013a). Mechanism and relevance of EWS/FLI-mediated transcriptional repression in Ewing sarcoma. Oncogene 32, 5089–5100.
Sankar S, Lessnick SL (2011). Promiscuous partnerships in Ewing's sarcoma. Cancer Genet 204, 351–365.
Sankar S, Tanner JM, Bell R, Chaturvedi A, Randall RL, Beckerle MC, Lessnick SL (2013b). A novel role for keratin 17 in coordinating oncogenic transformation and cellular adhesion in Ewing sarcoma. Mol Cell Biol 33, 4448–60.
Scotlandi K, Benini S, Manara MC, Serra M, Nanni P, Lollini PL, Nicoletti G, Landuzzi L, Chano T, Picci P, *et al*. (2000). Murine model for skeletal metastases of Ewing's sarcoma. J Orthop Res 18, 959–966.
Smilenov LB, Mikhailov A, Pelham RJ, Marcantonio EE, Gundersen GG (1999). Focal adhesion motility revealed in stationary fibroblasts. Science 286, 1172–1174.
Smith MA, Blankman E, Gardel ML, Luettjohann L, Waterman CM, Beckerle MC (2010). A zyxin-mediated mechanism for actin stress fiber maintenance and repair. Dev Cell 19, 365–376.
Smith R, Owen LA, Trem DJ, Wong JS, Whangbo JS, Golub TR, Lessnick SL (2006). Expression profiling of EWS/FLI identifies NKX2.2 as a critical target gene in Ewing's sarcoma. Cancer Cell 9, 405–416.
Spraker HL, Price SL, Chaturvedi A, Schiffman JD, Jones KB, Lessnick SL, Beckerle M, Randall RL (2012). The clone wars—revenge of the metastatic rogue state: the sarcoma paradigm. Front Oncol 2, 2.
Stupack DG, Puente XS, Boutsaboualoy S, Storgard CM, Cheresh DA (2001). Apoptosis of adherent cells by recruitment of caspase-8 to unligated integrins. J Cell Biol 155, 459–470.
Tirado OM, Mateo-Lozano S, Villar J, Dettin LE, Llort A, Gallego S, Ban J, Kovar H, Notario V (2006). Caveolin-1 (CAV1) is a target of EWS/FLI-1 and a key determinant of the oncogenic phenotype and tumorigenicity of Ewing's sarcoma cells. Cancer Res 66, 9937–9947.

Tirode F, Laud-Duval K, Prieur A, Delorme B, Charbord P, Delattre O (2007). Mesenchymal stem cell features of Ewing tumors. Cancer Cell 11, 421–429.
Truong H, Danen EH (2009). Integrin switching modulates adhesion dynamics and cell migration. Cell Adh Migr 3, 179–181.
Turc-Carel C, Aurias A, Mugneret F, Lizard S, Sidaner I, Volk C, Thiery JP, Olschwang S, Philip I, Berger MP, *et al.* (1988). Chromosomes in Ewing's sarcoma. I. An evaluation of 85 cases of remarkable consistency of t(11;22)(q24;q12). Cancer Genet Cytogenet 32, 229–238.
Vormoor B, Knizia HK, Batey MA, Almeida GS, Wilson I, Dildey P, Sharma A, Blair H, Hide IG, Heidenreich O, *et al.* (2014). Development of a preclinical orthotopic xenograft model of Ewing sarcoma and other human malignant bone disease using advanced in vivo imaging. PLoS One 7, e85128.
Wang YX, Mandal D, Wang S, Hughes D, Pollock RE, Lev D, Kleinerman E, Hayes-Jordan A (2009). Inhibiting platelet-derived growth factor beta reduces Ewing's sarcoma growth and metastasis in a novel orthotopic human xenograft model. In Vivo 23, 903–909.
Wiles ET, Bell R, Thomas D, Beckerle MC, Lessnick SL (2013). ZEB2 represses the epithelial phenotype and facilitates metastasis in Ewing sarcoma. Genes Cancer 4, 486–500.
Yoshigi M, Hoffman LM, Jensen CC, Yost HJ, Beckerle MC (2005). Mechanical force mobilizes zyxin from focal adhesions to actin filaments and regulates cytoskeletal reinforcement. J Cell Biol 171, 209–215.
Zaidel-Bar R, Itzkovitz S, Ma'ayan A, Iyengar R, Geiger B (2007). Functional atlas of the integrin adhesome. Nat Cell Biol 9, 858–867.